Chemical Science

ROYAL SOCIETY OF CHEMISTRY

EDGE ARTICLE

View Article Online
View Journal | View Issue

Cite this: *Chem. Sci.*, 2024, **15**, 15432

All publication charges for this article have been paid for by the Royal Society of Chemistry

Received 12th July 2024
Accepted 28th August 2024

DOI: 10.1039/d4sc04641b

rsc.li/chemical-science

Highly elastic relaxor ferroelectric *via* peroxide crosslinking†

Liang Gao,[ab] Linping Wang [a] and Ben-Lin Hu *[ab]

Relaxor ferroelectrics are well-known for their high dielectric constants, low dielectric losses, and excellent electromechanical properties, making them valuable for various electronic devices. Despite recent efforts to enhance the durability of ferroelectrics through chemical cross-linking, achieving elasticity in relaxor ferroelectric materials remains a significant challenge. These materials inherently possess traits such as low crystallinity and small crystal size, while chemical crosslinking tends to diminish polymer crystallinity considerably. Thus, a key obstacle to making relaxor ferroelectric polymers elastic lies in safeguarding their crystalline regions from the effects of slight crosslinking. To tackle this issue, we selected P(VDF-CTFE-DB) with highly reactive C=C double bonds as crosslinking sites, reducing the amount of cross-linking agents added and thereby lessening their impact on crystallinity. Through peroxide crosslinking, we transformed linear P(VDF-CTFE-DB) into a network structure, successfully producing a resilient relaxor ferroelectric material with maintained polarization intensity for ferroelectricity. Notably, this elastic relaxor ferroelectric was synthesized at relatively low temperatures, exhibiting a remarkable dielectric constant, superior resilience, fatigue resistance, and a stable ferroelectric response even under strains of up to 80%. Our approach paves the way for developing low-cost, high-dielectric-constant elastomers suitable for wearable electronics and related applications.

Introduction

Relaxor ferroelectrics (RFEs) possess vast potentials in contemporary electronic devices, particularly within the realm of flexible electronics, designated as the preferred materials for numerous electronic components, including acoustic sensors, solid-state coolers, transducers, and actuators. This preference stems from their exceptional properties, including high dielectric constant, low hysteresis, and superior electromechanical and pyroelectric properties.[1–5] Therefore, numerous efforts have been made to explore new methods, such as 'ferroelectric chemistry' to advance the synthesis of novel ferroelectrics.[6–8] Classic relaxor ferroelectrics, such as PMN-PT, exhibit diffuse phase transitions and strong frequency-dependent dielectric properties, making them highly suitable for applications in actuators, sensors, and transducers due to their large electro-mechanical coupling and high piezoelectric coefficients. The emergence of wearable electronics has propelled the demand for the elastification of functional materials,[9–12] leading us to develop elastic polymer ferroelectrics capable of delicately balancing crystallinity and resilience by slight crosslinking.[13] During the elastification wave of functional materials, relaxor ferroelectrics have lagged behind.[14,15] Polymer-based relaxor ferroelectric materials, such as the poly(vinylidene fluoride) (PVDF)-based terpolymers or tetrapolymers, have emerged as the premier choice for rendering relaxor ferroelectric materials elastic, due to their solution processability, chemical stability, and high flexibility.[16–19] Currently, significant strides have been made in elucidating the fundamental mechanisms underlying PVDF-based relaxor ferroelectric materials, thereby guiding the discovery of new relaxor ferroelectric organic materials for flexible, scalable, biocompatible sensor and energy applications.[20] The elastification of relaxor ferroelectric polymers holds profound importance and warrants comprehensive investigation, given its pivotal role in wearable or flexible electronics. However, the high cost of PVDF terpolymers or tetrapolymers, combined with their inherent challenges of low crystallinity and small crystal domains,[21] presents a dual challenge involving cost consideration and the intricate balancing between crystallinity and ferroelectricity in the elastification process of relaxor ferroelectric polymers.

To address the challenge, we meticulously selected a PVDF-based polymer, P(VDF-CTFE-DB),[22,23] as the starting material for several reasons. Firstly, P(VDF-CTFE) is highly cost-effective compared to other PVDF-based copolymers, with its cost being less than one percent of that of commonly used relaxor ferroelectric polymers like P(VDF-TrFE-CFE) (Table S1†). Secondly, the molecular structure of P(VDF-CTFE-DB) incorporates unsaturated –C=C– bonds, which not only simplifies the synthesis

[a]*Research Center for Advanced Interdisciplinary Sciences, Ningbo Institute of Materials Technology and Engineering, Chinese Academy of Sciences, Ningbo 315201, China. E-mail: hubenlin@nimte.ac.cn*

[b]*College of Materials Science and Opto-Electronic Technology, University of Chinese Academy of Sciences, Beijing 100049, China*

† Electronic supplementary information (ESI) available. See DOI: https://doi.org/10.1039/d4sc04641b

process but also significantly enhances reactivity and crosslinking efficiency.[24] Lastly, the synthesis of P(VDF-CTFE-DB) from the affordable P(VDF-CTFE) involves only a single-step reaction in a basic environment using triethylamine.[22] This straightforward synthesis, coupled with simple separation, is highly suitable for industrial scale-up.

In our previous work, the thermal crosslinking process requires high temperatures of up to 240 °C,[13] posing an additional high risk for CMOS or organic electronic procedures.[25–27] Thus, there is an urgent quest for alternative methods that operate under milder conditions to realize the elastification of ferroelectrics,[28,29] Herein, we intentionally opted for peroxide crosslinking, motivated by three key considerations. Firstly, the crosslinking temperature can be decreased by choosing suitable and active peroxides.[30] Secondly, peroxide crosslinking relies on highly reactive free radicals, ensuring high crosslinking efficiency, thus requiring lower additive amounts for efficient crosslinking.[31,32] Thirdly, the films prepared from peroxide crosslinking usually exhibit high thermal stability and excellent chemical stability due to their dense network structure.[33,34]

Bis(tert-butyldioxyisopropyl)benzene (BIPB) was selected as the initiator for the crosslinking due to its multifaceted advantages. This choice facilitates a reduction in additive amounts, along with offering high thermal decomposition activation energy, a slow decomposition rate, and the production of high-quality crosslinked products, minimal release of irritating odors, contributing to environmental friendliness.[35,36] Additionally, triallyl isocyanurate (TAIC) was chosen as the co-crosslinking agent to enhance crosslinking efficiency. As the best co-crosslinking agent, the triazine ring in TAIC imparts strong chemical and thermal stability, reinforcing the crosslinking network and further improving the thermodynamic and chemical stability of the crosslinked samples.[31,32,37]

Herein, a relaxor ferroelectric elastomer (crosslinked-P(VDF-CTFE-DB)) was successfully prepared by peroxide crosslinking at low temperatures (160 °C), exhibiting a high elastic recovery, high-dielectric constant, superior chemical and thermal stability, and cost-effectiveness. The resulting relaxor ferroelectric displays a high dielectric constant (approximately 22 at room temperature and 100 Hz), and a broad ferroelectric-to-paraelectric transition temperature range, indicating its capacity to maintain high dielectric constant across various temperature ranges. Moreover, this crosslinked P(VDF-CTFE-DB) film maintains a stable ferroelectric response even under strains up to 80%. In particular, compared to commercial fluorubbers, it exhibits superior resilience and fatigue resistance. By employing the peroxide initiator BIPB and the co-crosslinking agent TAIC, we obtained relaxor ferroelectric elastomers with high resilience and high dielectric constants at room temperature under a mild crosslinking condition.

Results and discussion

Preparation of elastic polymer RFEs *via* peroxide crosslinking

The polymer P(VDF-CTFE-DB) was synthesized following the reported method,[22] and its ^{1}H NMR spectrum in acetone-d_6 is shown in Fig. S1.† The pristine P(VDF-CTFE-DB) was dissolved in acetone, with a certain ratio of BIPB and TAIC. The resulting solution was then either cast or spin-coated onto substrates to form thick and thin films, respectively. After natural evaporation of the solvent in a fume hood, the blended P(VDF-CTFE-DB) was obtained with any residual solvent completely removed under vacuum. Subsequently, thermal crosslinking was conducted by step-heating in ambient air to gain the crosslinked P(VDF-CTFE-DB).

The crosslinking mechanism is illustrated in Fig. 1. Upon heating, the peroxide bonds in BIPB undergo homolytic

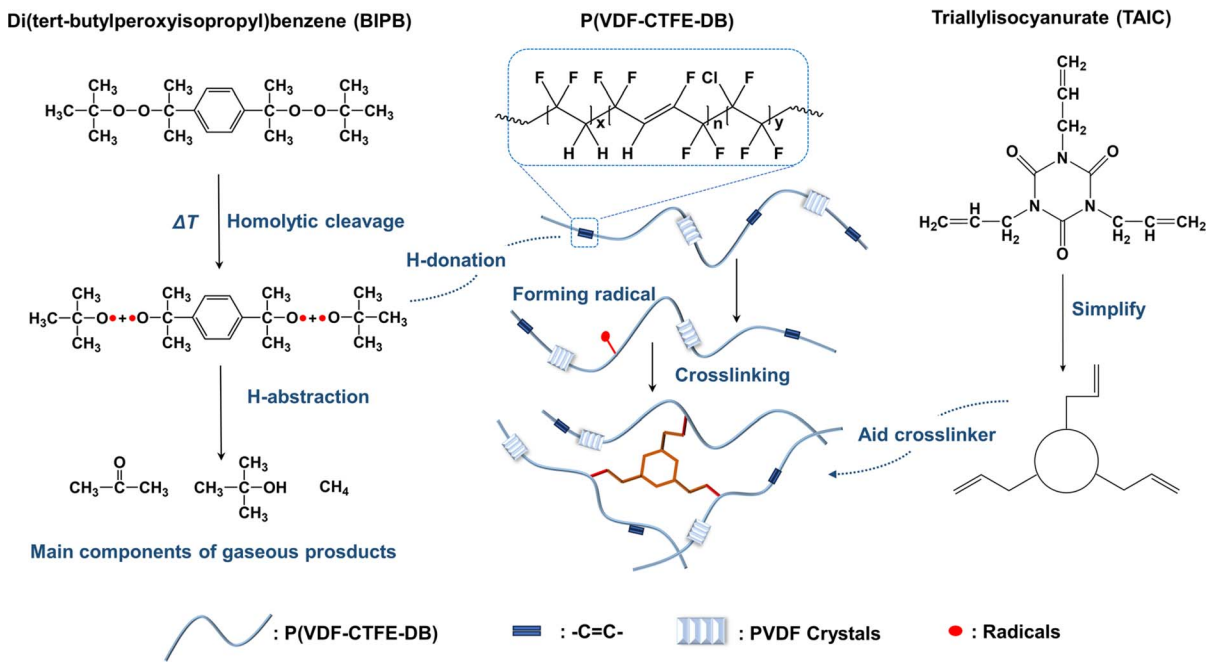

Fig. 1 The formation mechanism of elastic polymer ferroelectric by peroxide crosslinking.

cleavage, yielding alkoxyl free radicals.[31,32,38] These radicals subsequently initiate the attack on unsaturated C=C bonds within the PVDF-based polymer, generating polymer free radical intermediates. Interaction between these intermediates and the allylic bonds present in the tri-functional TAIC initiates the crosslinking reaction. Notably, TAIC played a crucial role as the co-crosslinking agent, facilitating the formation of the network with higher crosslinking density even at low BIPB feeding amounts.[37] Throughout this crosslinking process, by-products such as acetone, butanol, and methane were released in gaseous form.

Crosslinking and characterization of elastic RFE films

Through differential scanning calorimetry (DSC) analysis of the blended P(VDF-CTFE-DB) films illustrated in Fig. 2a, an exothermic peak corresponding to the crosslinking reaction is observed within the range of 120–215 °C. To ensure thorough crosslinking, thermal treatment at 160 °C for one hour was employed, resulting in complete crosslinking, as confirmed by the absence of an exothermic peak during the first heating cycle of the DSC curve (the inset of Fig. 2a) for the crosslinked P(VDF-CTFE-DB) film. Subsequently, DSC testing was conducted on crosslinked P(VDF-CTFE-DB) films with varying ratios of BIPB and TAIC, as shown in Fig. S2.† It is observed that the content of the crosslinking initiator within this range had no significant impact on the melting temperature of the crosslinked P(VDF-CTFE-DB) film. Nevertheless, as the ratio of the BIPB and TAIC increased, the crystalline melting enthalpy of the crosslinked P(VDF-CTFE-DB) film consistently decreased. It reaches an extremum at a peroxide initiator ratio of 10%, indicating enhanced crystallinity at this point—a crucial assurance for a favorable ferroelectric relaxor response, as illustrated in Fig. 2b.

The crosslinked P(VDF-CTFE-DB) films exhibited excellent thermal and chemical stability. Specifically, the crosslinked P(VDF-CTFE-DB) film demonstrated exceptional thermal stability, with a temperature of decomposition (T_d) exceeding 400 °C, as evidenced by the thermogravimetric analysis curve (Fig. S3†). Additionally, when subjected to various organic solvents such as acetone, cyclohexanone, isophorone, and DMF, the crosslinked P(VDF-CTFE-DB) films displayed stability, as shown in Fig. S4.† After immersion in these solvents for two weeks, minimal swelling was observed, and the gel contents remained around 90%, as presented in Table S2.† Moreover, in subsequent acid–base resistance tests, no obvious color or volume changes were observed in the crosslinked P(VDF-CTFE-DB) films after two weeks of immersion in concentrated sulfuric acid and saturated sodium hydroxide aqueous solution, as depicted in Fig. S5.† These findings highlight the enhanced stability of electronic devices fabricated using crosslinked

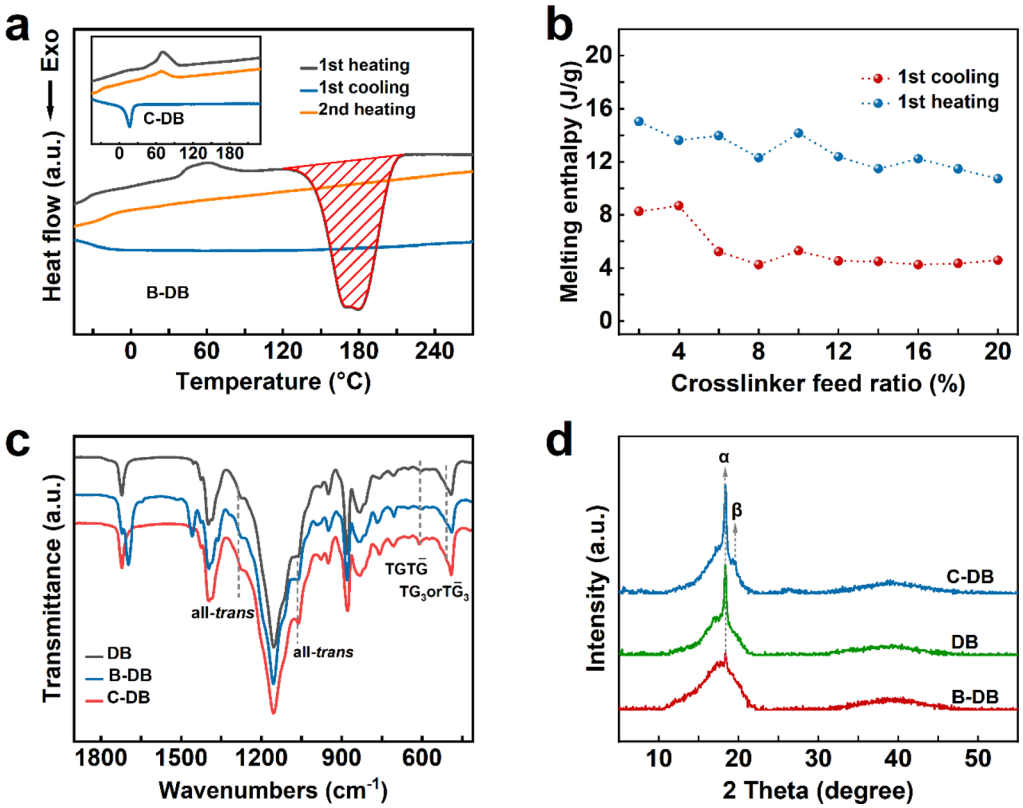

Fig. 2 Crosslinking characterization of elastic RFE films with the ratios of BIPB and TAIC is 10% and 8%, respectively. (a) DSC curves of the blended P(VDF-CTFE-DB) ('B-DB' for short) film indicating *in situ* crosslinking. (Inset) DSC curves of the crosslinked P(VDF-CTFE-DB) ('C-DB' for short). (b) Melting enthalpy of crosslinked P(VDF-CTFE-DB) films with different crosslinking densities. (c and d) FT-IR spectra (c) and XRD patterns (b) of pristine ('DB' for short), blended and crosslinked P(VDF-CTFE-DB) films.

P(VDF-CTFE-DB) films, thereby expanding their potential applications.

Fourier-transform infrared spectroscopy (FT-IR) analysis revealed structural changes in the films pre- and post-crosslinking, as shown in Fig. 2c. In the blended P(VDF-CTFE-DB) film, the disappearance of the C=C double bond signal of the crosslinking agent TAIC at ~1697 cm^{-1} after crosslinking suggests its extensive involvement during the crosslinking reaction. Notably, the C=C double bonds within the P(VDF-CTFE-DB) chain did not fully participate in the crosslinking process, as evidenced by the persistent presence of C=C double bonds at 1720 cm^{-1} (Fig. S6a†). After crosslinking, there was a notable increase in the content of the α-phase (610 cm^{-1}) and β-phase (1060 cm^{-1}), particularly in the α-phase, as observed in Fig. S6b–S6d.† This finding was further confirmed by X-ray diffraction (XRD) analysis (Fig. 2d), which demonstrated an increased content of α-phase (18.9°) and β-phase (19.2°) after crosslinking.[39]

Further insights were gained into the significant influence of the content of BIPB and TAIC on the mechanical properties of the crosslinked P(VDF-CTFE-DB) films. Stress–strain tests were conducted on crosslinked P(VDF-CTFE-DB) films with varying ratios of the peroxides, as depicted in Fig. 3. When comparing to the pristine P(VDF-CTFE-DB) film lacking a crosslinking initiator (Fig. S7†), the elongation at break sharply decreased from ~1300% for the pristine P(VDF-CTFE-DB) to ~340% for the crosslinked P(VDF-CTFE-DB) with a BIPB ratio of 2%. As the content of the BIPB and TAIC increased, a decreasing trend in the elongation at break was observed, alongside an increasing trend in modulus, as shown in Fig. 3b. Furthermore, cyclic stress–strain tests were conducted on crosslinked P(VDF-CTFE-DB) films with initiator ratios of 8% and 10% (refer to Fig. S8†), indicating superior cyclic performance for the films with a 10% BIPB ratio. Based on the comprehensive results of mechanical properties and crystalline melting enthalpy, the 10% initiator ratio was deemed more suitable for achieving a balance between elasticity and crystallinity, thus using it as the preferred ratio for all subsequent experiments.

Further cyclic stress–strain testing was performed, comprising 5 cycles (depicted in Fig. 3c) and an extended 3000 cycles (illustrated in Fig. 3d). The results indicated that the recovery rate of the film remained consistently above 95% under strains ranging from 40% to 80% during cyclic loading. Compared to commercial fluorubber, the crosslinked P(VDF-CTFE-DB) film exhibited superior fatigue resistance and higher recovery ratios. Remarkably, even after 100 cycles, the crosslinked P(VDF-CTFE-DB) film promptly maintained stable elastic recovery. To decipher the underlying mechanism behind the film's elasticity, stress–temperature performance testing was conducted on the crosslinked P(VDF-CTFE-DB) films. The elasticity of the crosslinked P(VDF-CTFE-DB) film, as determined by varying the temperature under different strains

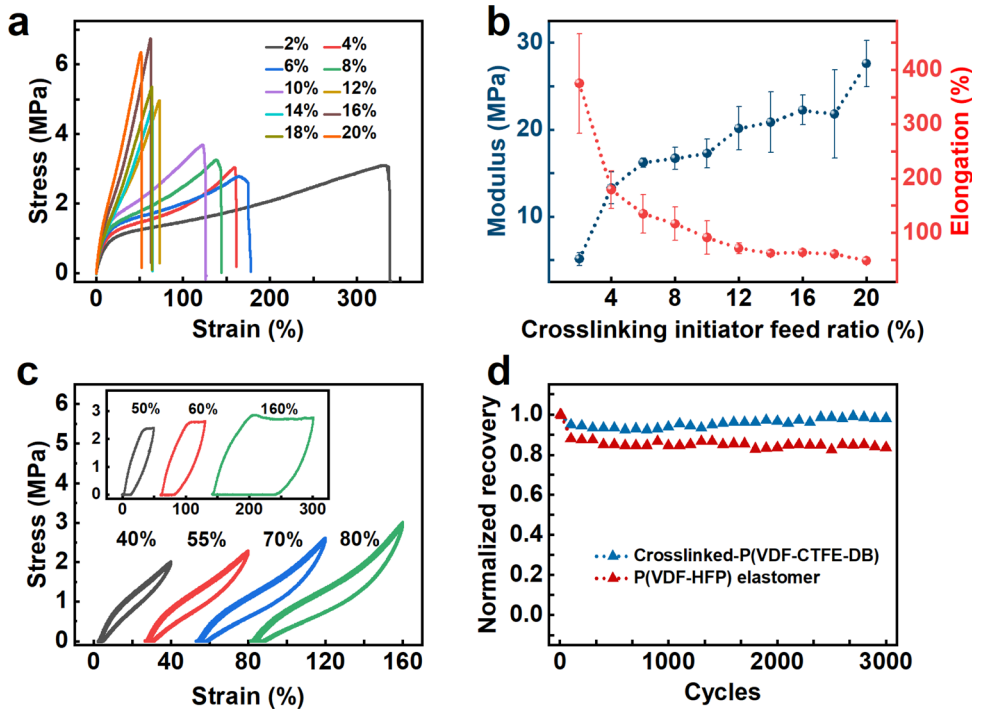

Fig. 3 Mechanical properties of elastic RFE films. (a) Stress–strain curves of crosslinked P(VDF-CTFE-DB) films at various crosslinking initiator ratios. (b) Modulus and elongation of crosslinked P(VDF-CTFE-DB) films at various crosslinking initiator ratios. (c) Cyclic stress–strain curves of crosslinked P(VDF-CTFE-DB) films with a crosslinking initiator ratio of 10% and pristine P(VDF-CTFE-DB) films (inset) under different strains (the first cycle was omitted owing to clamp sliding and the *X*-axis is shifted for clarity), indicating the excellent resilience of the crosslinked P(VDF-CTFE-DB) films compared with the unrecoverable deformation of the pristine P(VDF-CTFE-DB) films. (d) The fatigue resistance of crosslinked P(VDF-CTFE-DB) film with a crosslinking density of 10% under 50% strain, compared to that of a commercial fluorubber P(VDF-HFP) (DAI-EL, G-801).

(Fig. S9†), was attributed to entropy elasticity rather than energy elasticity.[13] This inherence arises from the transformation of macromolecular chain conformations within the crosslinked P(VDF-CTFE-DB) film from coil-like to rod-like shape under external forces, resulting in a decrease in the entropy change. The rod-like state of the system becomes unstable, and upon removal of the external force, due to thermal motion, the molecular chains spontaneously tend toward an increase of the entropy change in the system. Consequently, the molecular chains revert from the rod-like shape to the coil-like shape, exhibiting excellent elastic recovery properties.[40–43] These results confirm that the intrinsic elasticity of relaxor ferroelectric polymers is achieved through peroxide initiation at a relatively low temperature.

Relaxor ferroelectricity of crosslinked P(VDF-CTFE-DB)

The ferroelectric relaxor behavior of crosslinked P(VDF-CTFE-DB) is characterized using dielectric-temperature curves, polarization-electric field curves, and piezoresponse force microscopy (PFM) testing, as illustrated in Fig. 4.

The dielectric–temperature curve of the crosslinked P(VDF-CTFE-DB) film reveals distinct relaxor characteristics with a broader Curie transition temperature (T_c) range. As the test frequency increases, the T_c shifts towards higher temperatures, enabling the crosslinked P(VDF-CTFE-DB) film to possess a higher dielectric constant near room temperature. Notably, both the T_c and the peak temperature of dielectric loss shift towards higher temperatures with increasing frequency, demonstrating significant frequency dependence. Compared to pristine P(VDF-CTFE-DB) (Fig. S10†), the crosslinked film exhibits a higher dielectric constant and a wider range of low dielectric loss temperatures. At room temperature and under a frequency of 100 Hz, the dielectric constant reaches approximately 22, with a dielectric loss tangent below 0.1 (Fig. 4a). The Vogel–Fulcher relationship is employed to describe the dynamics of thermally activated dipoles and the freezing behavior of relaxor ferroelectrics. It reflects the freezing behavior caused by the interaction between dipoles. The Vogel–Fulcher relation as shown in eqn (1) (ref. 44)

$$f = f_0 \exp\left[\frac{E_a}{k_B/T_{max} - T_{VF}}\right] \quad (1)$$

where E_a is the activation energy, f is the probing frequency k_B is the Boltzmann constant (8.617×10^{-5} eV k^{-1}), f_0 is the relaxation frequency of dipoles, T_f is the freezing temperature, and T_m is the temperature corresponding to the maximum dielectric constant. Vogel–Fulcher equation fits of our permittivity data measured for frequencies ranging between 100 Hz and 1 MHz are given in Fig. S11.† They show the predicted linear relation between the reduced frequency $[\ln(f/f_0)]^{-1}$ and T_{max}. All fitting parameters are consistent with the Vogel–Fulcher law. Intrinsic elastomers with such high dielectric constant and low dielectric loss are the key materials for soft robots and wearable devices, serving as elastic sensors, energy storage units, and actuators.

The P–E loops of crosslinked P(VDF-CTFE-DB) were obtained using a sandwich structure device (Au/C-DB/Au/Si). As shown in Fig. 4b, the loops exhibited a low rectangularity, appearing slender, which is a typical feature of a relaxor ferroelectric material. As the applied electric field increases, the initial hysteresis does not gradually expand but maintains a slender shape, characterized by a significantly large ratio between saturated polarization (P_{max}) and remanent polarization (P_r),

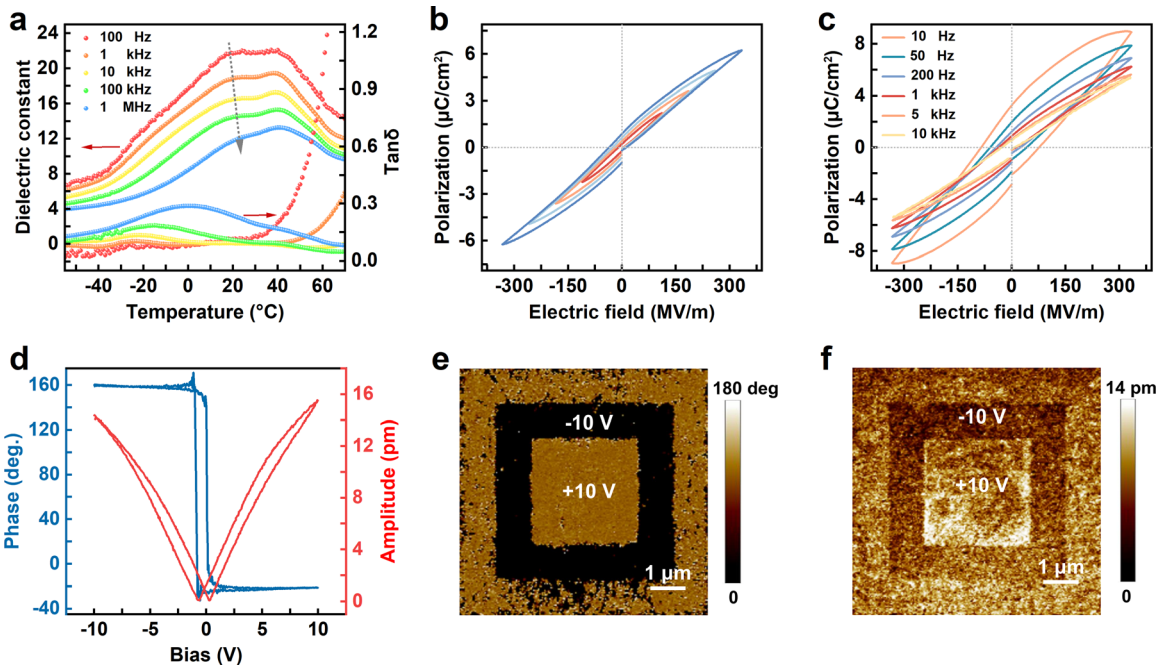

Fig. 4 Ferroelectric properties of crosslinked P(VDF-CTFE-DB) films. (a) Temperature-dependent ε and dielectric loss of crosslinked P(VDF-TrFE-DB) films at different frequencies. (b and c) P–E loops of Au/C–P(VDF-CTFE-DB)/Au under different electric fields at 1000 Hz (b) and different frequencies (c). (d) Phase-voltage hysteresis and amplitude–voltage butterfly loop. (e and f) phase (e) and amplitude (f) mapping of PFM.

resulting in lower rectangularity. At 1 kHz and 330 MV m^{-1}, the P_{max} and P_r of the crosslinked P(VDF-CTFE-DB) film are 6.23 and 0.87 μC cm^{-2}, respectively. In comparison, the pristine P(VDF-CTFE-DB) exhibits P_{max} and P_r values of 3.32 and 0.52 μC cm^{-2}, respectively (Fig. S12a†). The coercive field (E_c) of ~36 MV m^{-1} remains unchanged before and after crosslinking. However, as the applied electric field continues to increase, both P_{max} and P_r continue to grow, exhibiting a saturating trend. Eventually, at a high electric field of 880 MV m^{-1}, P_{max} and P_r reach 14 and 4.5 μC cm^{-2}, respectively, with a coercive field E_c of approximately 177 MV m^{-1} (Fig. S13†). This demonstrates a pronounced saturation trend, highlighting the saturated characteristics of relaxor ferroelectric material under a strong electric field. The P_r of the crosslinked P(VDF-CTFE-DB) increases from 0.51 to 3.23 μC cm^{-2} across test frequencies ranging from 10 kHz to 10 Hz (Fig. 4c). Compared to pristine P(VDF-CTFE-DB) (Fig. S10b†), the crosslinked P(VDF-CTFE-DB) film exhibits more pronounced relaxor behavior due to a more condensed network introduced by peroxide crosslinking. The introduction of C=C double bonds in the ferroelectric polymer reduces spatial hindrance for ferroelectric phase formation and promotes the generation of the ferroelectric phase. This enhancement is partly attributed to the increase in both the non-polar α-phase and the polar β-phase. In addition, the enhanced polarization effect at the interface resulting from the crosslinked network structure also contributes to polarization. However, the polarization at the interface cannot persist after the removal of the electric field, leading to a significant increase in saturated polarization while P_r undergoes minimal changes, thereby enhancing the relaxor behavior of the crosslinked P(VDF-CTFE-DB).

We utilized PFM to investigate the phase and amplitude changes of crosslinked P(VDF-CTFE-DB) under the stimuli of positive and negative electric fields,[45] confirming the excellent piezoelectric properties of the crosslinked P(VDF-CTFE-DB) film (Fig. 4d–f). A 250 nm-thick film was spin-coated on a Pt/Si substrate, and after crosslinking, PFM electrically conductive probes were utilized for ferroelectric property testing. Hysteresis and butterfly curves obtained from a single scan demonstrate the complete switching of ferroelectric domains under the influence of the electric field (Fig. 4d). By applying a −10 V bias to a 5 × 5 $μm^2$ region, maintaining the same center, and subsequently applying a +10 V bias to a 3 × 3 $μm^2$ region, phase and amplitude maps of a "box-in-box" pattern were obtained (Fig. 4e and f), suggesting that the polarity of the ferroelectric domains in the crystalline can be reversibly switched by applied field in a zone rather than only a spot. Additionally, PFM reveals a piezoelectric coefficient of 10.7 pm V^{-1} (Fig. S14†), which is a typical value for PVDF-based ferroelectric polymers.

Relaxor ferroelectricity response of crosslinked P(VDF-CTFE-DB) under strains

A fully elastic capacitor device, utilizing liquid metal (Ga, gallium) as elastic electrodes, was fabricated using a sacrificial-layer microfabrication method to investigate the relaxor ferroelectric response of the crosslinked P(VDF-CTFE-DB) film under

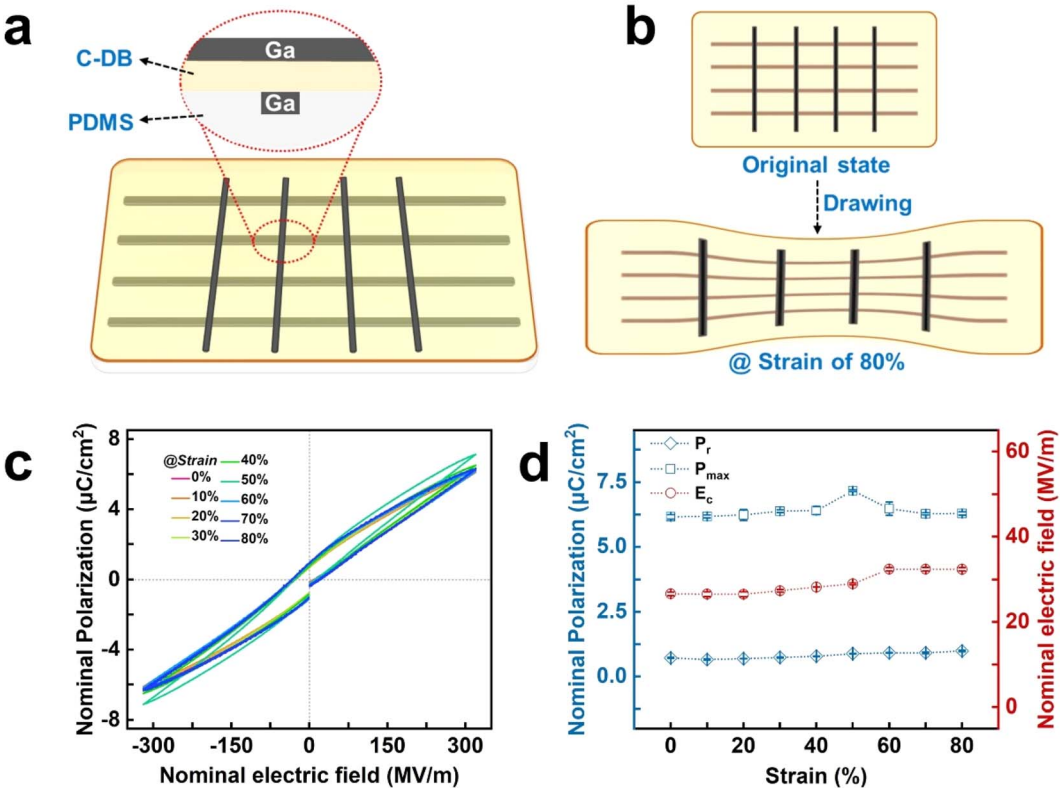

Fig. 5 FE response of elastic RFEs under strains. (a and b) Schematic structure of elastic device (a) in the stretching set-up under 0 and 80% strain (b). (c) *P*–*E* loops at 1 kHz under strain from 0 to 80%. (d) P_r, P_{max}, and E_c under different strains.

various applied strains and frequencies.[16] The schematic structure of the elastic device is illustrated in Fig. 5a. The elastic device was affixed in a custom-made single-shaft tensile clamp and gradually stretched to 80% strain, as depicted in Fig. 5b. The test results are summarized in Fig. 5c,d.

The *P*–*E* loops of this fully elastic device (Fig. S15 and 16†) without strain are similar to that of the rigid device with Au electrodes, and the P_r remains almost constant throughout the stretching process (Fig. S17–S24†). Although there is a slight fluctuation in the P_{max} during stretching, the coercive electric field remains nearly constant within the 0–40% strain range. However, it begins to fluctuate when the strains reach 40–60% and remain stable again in the 60–80% strain range. These observations suggest that the RFE response of the elastic relaxor ferroelectrics is insensitive to stress and frequency.

Intrinsic elastomer with high dielectric constants for wearable electronics

High-dielectric-constant elastomers are crucial components in emerging wearable electronics, such as non-volatile memory, energy-storage devices and fully elastic circuits.[46,47] The elastomers for wearable electronics will undergo large strains (the maximum up to 30–50%) at high frequencies (0.1–100 Hz), therefore, they require high resilience (elastic recovery, fatigue resistance), excellent electrical performance (high dielectric constant and low loss, high break-down electric field), and efficient solution-processability.[48] In addition, cost-effectiveness is also a primary consideration for materials used in wearable electronics, given their status as daily consumables with a massive demand for consumption. However, the properties of current intrinsic elastomers fall short of the above requirements. For example, the dielectric constant of the most commonly used PDMS elastomer in wearable devices is just 2.8 at 1 kHz, and even the best dielectric elastomers have a range of 3–8.[49] Therefore, it is urgent to develop intrinsic elastomers with high dielectric constant and low loss, robust elastic properties at low cost.

Compared to PDMS and other reported intrinsic elastomers, our crosslinked P(VDF-CTFE-DB) exhibits a dielectric constant of ~20 at 1 kHz, which is the highest value among all reported intrinsic elastomers. The resilience of crosslinked P(VDF-CTFE-DB) is also as excellent as PDMS and surpasses most reported dielectric elastomers. Even compared with commercial PVDF ternary polymer materials, our material is not only cost-effective but also exhibits a low modulus and high resilience (Fig. S25†). One of the most notable advantages of our cross-linked P(VDF-CTFE-DB) is its cost, which is less than 1% of that of P(VDF-TrFE) and PVDF-based terpolymers. Above all, the outstanding performance of our crosslinked P(VDF-CTFE-DB) films significantly broadens the potential application scenarios of organic relaxor ferroelectric materials.

Conclusions

Through a successful free-radical crosslinking reaction at relatively low temperatures, we have synthesized relaxor ferroelectric materials exhibiting high elastic recovery while retaining their ferroelectricity. This material features a relatively high dielectric constant (~22 at 100 Hz) and a low modulus (~10 MPa), which is the highest value among all reported intrinsic elastomers. In addition, the superior resilience and fatigue resistance of our elastomer is better than that of commercial fluorubbers. It demonstrates outstanding stability in organic solvents, strong acids, and strong bases. Even under strains as high as 80%, it maintains a stable ferroelectric response. Our strategy provides a novel approach to the elastification of relaxor ferroelectric materials, offering a new elastomer for applications in the field of flexible electronics, such as soft robotics and elastic electronic skin.

Data availability

The data supporting this article have been included as part of the ESI.†

Author contributions

B. L. H. conceived this study. L. G. wrote the draft. L. G., L. P. W. and B. L. H. designed the experiments, analyzed the results, and revised the manuscript. All authors have given approval to the final version of the manuscript.

Conflicts of interest

There are no conflicts to declare.

Acknowledgements

This work is supported by Zhejiang Provincial Natural Science Foundation of China (LR24E030003), Zhejiang Province Qianjiang Talent Program (ZJ-QJRC-2020-32).

Notes and references

1 L.-E. Cross, S.-J. Jang, R.-E. Newnham, S. Nomura and K. Uchino, *Ferroelectrics*, 1980, **23**, 187–191.
2 Q.-M. Zhang, V. Bharti and X. Zhao, *Science*, 1998, **280**, 2101–2104.
3 Z. Kutnjak, J. Petzelt and R. Blinc, *Nature*, 2006, **441**, 956–959.
4 Z. Zhang, X. Wang, S. Tan and Q. Wang, *J. Mater. Chem. A*, 2019, **7**, 5201–5208.
5 X. Qian, X. Chen, L. Zhu and Q.-M. Zhang, *Science*, 2023, **380**, eadg0902.
6 W.-Q. Liao, D. Zhao, Y. Tang, Y. Zhang, P. Li, P. Shi, X. Chen, Y. You and R.-G. Xiong, *Science*, 2019, **363**, 1206–1210.
7 H. Liu, H. Zhang, X. Chen and R.-G. Xiong, *J. Am. Chem. Soc.*, 2020, **142**, 15205–15218.
8 Y. You, W. Liao, D. Zhao, H. Ye, Y. Zhang, Q. Zhou, X. Niu, J. Wang, P. Li, D. Fu, Z. Wang, S. Gao, K. Yang, J. Liu, J. Li, Y. Yan and R.-G. Xiong, *Science*, 2017, **357**, 306–309.
9 J.-A. Rogers, T. Someya and Y. Huang, *Science*, 2010, **327**, 1603–1607.

10 Y. Jiang, Z. Zhang, Y. Wang, D. Li, C. Coen, E. Hwaun, G. Chen, H. Wu, D. Zhong, S. Niu, W. Wang, A. Saberi, J. Lai, Y. Wu, Y. Wang, A.-A. Trotsyuk, K.-Y. Loh, C. Shih, W. Xu, K. Liang, K. Zhang, Y. Bai, G. Gurusankar, W. Hu, W. Jia, Z. Cheng, R.-H. Dauskardt, G.-C. Gurtner, J.-B.-H. Tok, K. Deisseroth, I. Soltesz and Z. Bao, *Science*, 2022, **375**, 1411–1417.
11 D. Jung, C. Lim, H.-J. Shim, Y. Kim, C. Park, J. Jung, S.-I. Han, S. Sunwoo, K.-W. Cho, G.-D. Cha, D.-C. Kim, J.-H. Koo, J.-H. Kim, T. Hyeon and D. Kim, *Science*, 2021, **373**, 1022–1026.
12 Y. Zheng, Y. Liu, D. Zhong, S. Nikzad, S. Liu, Z. Yu, D. Liu, H. Wu, C. Zhu and J. Li, *Science*, 2021, **373**, 88–94.
13 L. Gao, B.-L. Hu, L. Wang, J. Cao, R. He, F. Zhang, Z. Wang, W. Xue, H. Yang and R.-W. Li, *Science*, 2023, **381**, 540–544.
14 H. Zhang and R.-G. Xiong, *Science*, 2023, **381**, 484–485.
15 B.-L. Hu, B. Dkhil and R.-W. Li, *Sci. Bull.*, 2023, **68**, 2691–2694.
16 X. Qian, X. Chen, L. Zhu and Q.-M. Zhang, *Science*, 2023, **380**, eadg0902.
17 X. Chen, H. Qin, X. Qian, W. Zhu, B. Li, B. Zhang, W. Lu, R. Li, S. Zhang, L. Zhu, F. D. D. Santos, J. Bernholc and Q.-M. Zhang, *Science*, 2022, **375**, 1418–1422.
18 T. Soulestin, V. Ladmiral, F.-D. D. Santos and B. Ameduri, *Prog. Polym. Sci.*, 2017, **72**, 16–60.
19 Z.-X. Wang and W.-Q. Liao, *Science*, 2022, **375**, 1353–1354.
20 Y. Liu, B. Zhang, W. Xu, A. Haibibu, Z. Han, W. Lu, J. Bernholc and Q. Wang, *Nat. Mater.*, 2020, **19**, 1169–1174.
21 L. Yang, X. Li, E. Allahyarov, P.-L. Taylor, Q.-M. Zhang and L. Zhu, *Polymer*, 2013, 1709–1728.
22 S. Tan, J. Li, G. Gao, H. Li and Z.-C. Zhang, *J. Mater. Chem.*, 2012, **22**, 18496–18504.
23 S. Tan, X. Hu, S. Ding, Z.-C. Zhang, H. Li and L. Yang, *J. Mater. Chem. A*, 2013, **1**, 10353–10361.
24 A. Smedberg, T. Hjertberg and B. Gustafsson, *Polymer*, 1997, **38**, 4127–4138.
25 A.-K.-K. Kyaw, F. Jamalullah, L. Vaithieswari, M.-J. Tan, L. Zhang and J. Zhang, *ACS Appl. Mater. Interfaces*, 2016, **8**, 9533–9539.
26 H.-J. Kim, A. Han, C. Cho, H. Kang, H. Cho, M.-Y. Lee, J.-M.-J. Fréchet, J.-H. Oh and B.-J. Kim, *Chem. Mater.*, 2012, **24**, 215–221.
27 J. Park, J.-W. Chung, J. Kim, J. Lee, J.-Y. Jung, B. Koo, B. Lee, S.-W. Lee, Y.-W. Jin and S.-Y. Lee, *J. Am. Chem. Soc.*, 2015, **137**, 12175–12178.
28 L. Wang, L. Gao, B. Li, B. Hu, T. Xu, H. Lin, R. Zhu, B.-L. Hu and R.-W. Li, *J. Am. Chem. Soc.*, 2024, **146**, 5614–5621.
29 B. Li, L. Wang, L. Gao, T. Xu, D. Zhang, F. Li, J. Lyu, R. Zhu, X. Gao, H. Zhang, B.-L. Hu and R.-W. Li, *Angew. Chem., Int. Ed.*, 2024, **63**, e202400511.
30 G. Kyselá, I. Hudec, P. Alexy and S. Bratislava, *Manufacturing and processing of rubber*, Slovak University of Technology Press, 2010.
31 J.-B. Finlay, A. Hallenbeck and J.-D. MacLachlan, *J. Elastomers Plastics*, 1978, **10**, 3–16.
32 G. Kojima and H. Wachi, *Rubber Chem. Technol.*, 1978, **51**, 940–947.
33 W. Naebpetch, B. Junhasavasdikul, A. Saetung, T. Tulyapitak and N. Nithi-Uthai, *Plast., Rubber Compos.*, 2016, **45**, 436–444.
34 J. Wang, S. Pan, Y. Zhang and S. Guo, *Polym. Test.*, 2017, **59**, 253–261.
35 Y. Ren, X. Sun, L. Chen, Y. Li, M. Sun, X. Duan and W. Liang, *RSC Adv.*, 2021, **11**, 6791–6797.
36 Y. Hao, J. Chen, Y. Liu, F. Wang, Q. Chen, W. Zhang, S. Zhang, W. Chen and H. Tian, *Iran. Polym. J.*, 2023, **32**, 1271–1280.
37 A. Simon, J. Pépin, M. Deffarges, S. Méo and D. Berthier, *European Conference of Constitutive Models for Rubbers (ECCMR2022)*, Milan, Italy, 2022.
38 Y. Jing, Z. Zhao, X. Cao, Q. Sun, Y. Yuan and T. Li, *Nat. Commun.*, 2023, **14**, 8060.
39 W. Xia and Z. Zhang, *IET Nanodielectr.*, 2018, **1**, 17–31.
40 M. Behl, M.-Y. Razzaq and A. Lendlein, *Adv. Mater.*, 2010, **22**, 3388–3410.
41 W. Liu, Y. Liu, G. Zeng, R. Liu and Y. Huang, *Polymer*, 2012, **53**, 1005–1014.
42 A. Bae, S. Lee, M. Ikeda, M. Sano, S. Shinkai and K. Sakurai, *Carbohydr. Res.*, 2004, **339**, 251–258.
43 K.-O. Kim and T. Choi, *ACS Macro Lett.*, 2012, **1**, 445–448.
44 D. Viehland, S.-J. Jang, L.-E. Cross and M. Wuttig, *J. Appl. Phys.*, 1990, **68**, 2916.
45 A. Gruverman, M. Alexe and D. Meier, *Nat. Commun.*, 2019, **10**, 1661.
46 Y. Shi, E. Askounis, R. Plamthottam, T. Libby, Z. Peng, K. Youssef, J. Pu, R. Pelrine and Q. Pei, *Science*, 2022, **377**, 228–232.
47 M. Duduta, E. Hajiesmaili, H. Zhao, R.-J. Wood and D.-R. Clarke, *Proc. Natl. Acad. Sci. U. S. A.*, 2019, **116**, 2476–2481.
48 T. Someya, Z. Bao and G.-G. Malliaras, *Nature*, 2016, **540**, 379–385.
49 G. Gallone, F. Carpi, D. De Rossi, G. Levita and A. Marchetti, *Mater. Sci. Eng. C*, 2007, **27**, 110–116.